Variations in Optical S^+ Emission from the Io Plasma Torus: Evidence for Quasiperiodicity

R. Carey Woodward, Jr.[1], Frank Scherb[1], and Fred L. Roesler[1]
University of Wisconsin—Madison, Physics Dept.

ABSTRACT

As part of its efforts to monitor and characterize periodic variations in the Io plasma torus, the Wisconsin Space Physics group acquired Fabry-Perot spectra of [S II] $\lambda\lambda$6716,6731 for a five-week period in 1988. Previous analysis (Woodward *et al.* 1994) showed periodicity, but, surprisingly, not at 10.2 hours—the persistent 3% subcorotational period, often called System IV, reported in other long-term torus data sets. We show here that our 1988 data exhibit a *quasiperiodic* intensity variation at 10.2 hours, characterized by two distinct intensity enhancements which abruptly changed in relative magnitude during the observational run. We also present perpendicular ion temperature data from the same period, showing a periodic variation anticorrelated with intensity after the aforementioned abrupt change, but no significant periodicity beforehand. This non/anticorrelation appears to eliminate the possibility that a slowly moving magnetic field enhancement is responsible for the subcorotational periodicity. Considering these and other long-term data, we suggest that the various observed subcorotational features are not themselves responsible for the 3% subcorotational period, but rather are independent features modulated or otherwise affected by a permanent, global phenomenon in the torus lagging corotation by 3%.

Subject headings: magnetic fields — planets and satellites: individual (Io, Jupiter) — plasmas

To appear in *The Astrophysical Journal*, vol. **479** (20 April 1997).
© 1996 The American Astronomical Society. All rights reserved.

---

[1]Visiting Astronomer, National Solar Observatory, National Optical Astronomy Observatories, which is operated by the Association of Universities for Research in Astronomy, Inc., under contract with the National Science Foundation

1. Introduction

One of the most intriguing phenomena of the Io plasma torus is the periodic variation of its emission intensities at several wavelengths and Jovicentric distances with a ~ 10.22 hour period: 3% slower than the expected System III period of 9.925 hours. This persistent, long-term corotational lag has been observed in groundbased near-IR [S III] λ9531 data at 5–7 R_J (Roesler *et al.* 1984), *Voyager* EUV S^{++},O^{++} 685Å data at 4–8 R_J (Roesler *et al.* 1984, Sandel and Dessler 1988), *Voyager* narrow-band kilometric (nKOM) radio data (originating mostly from 8–9 R_J) (Kaiser and Desch 1980, Daigne and Leblanc 1986, Yang and Dessler 1991), and more recently, in a six-month groundbased observing run of optical [S II] $\lambda\lambda$6716,6731 at 6–7 R_J (Brown 1995) and a reanalysis of *Voyager* hectometric radio data (Kaiser *et al.* 1996).

The Wisconsin space physics group has been been particularly interested in this subcorotational periodicity since discovering it in our 1982 observations of [S III] λ9531 emission (Roesler *et al.* 1984). In November and December 1988 we acquired a large set of high-spectral-resolution scans of [S II] $\lambda\lambda$6716,6731 and [S III] λ9531, primarily to study further this anomalous periodicity. We performed a careful periodicity analysis on our [S II] λ6731 intensity data, but found, to our surprise, that the data showed no periodic variation at 10.22 hours; instead, we found a statistically significant period of 10.14 ± 0.06 h (Woodward *et al.* 1994). During the course of analysis, we had noticed that the data could be described as organized in System IV if the first and last parts of the run were taken separately, but saw no reason so to separate the data. Brown (1995), however, recently reported finding a periodicity of 10.214 ± 0.006 hours in [S II] $\lambda\lambda$6716,6731 intensities, but only after excluding, at certain Jovicentric distances, a 22-day interval during which the same period was evident but with different phase. (Interestingly, when he does not exclude this interval, Brown finds a period of 10.16 h, in agreement with our earlier result.) We therefore re-examined our 1988 [S II] λ6731 intensity data and our previously unpublished 1988 [S II] $\lambda\lambda$6716,6731 temperature data, looking for similar behavior.

2. Observation and reduction

The observation and reduction of these data have already been described in Woodward (1992) and Woodward *et al.* (1994); the interested reader is referred there for details beyond the following summary.

The data consist of spectral scans taken with a dual-etalon Fabry-Perot interferometer on the main and east auxiliary telescopes at the McMath-Pierce Solar Telescope facility on Kitt Peak, through a 2.0 or 2.6 R_J diameter circular aperture centered on the east or west ansa of the plasma torus at a distance of 6 R_J from Jupiter. Because the data are scans, they contain no spatial information, but have superior spectral ($\Re \sim 25000$) and temporal (scan times ranging from 10 to 14 minutes) resolutions. The spectrometer sensitivity allowed the use of the small (0.81 m primary) east auxiliary telescope for the bulk of the observations; this in turn permitted us sufficient telescope time to acquire data with the long timebase necessary for a proper periodicity search.

We acquired 157 scans of [S II] λ6731 and 39 scans of [S II] λ6716 (along with scans at other wavelengths, broadband images, and datacubes) during 22 nights over a 36 day (87 Jovian rotation) period—considerably less than we had hoped for, but adequate for a periodicity search. The scans were separated by intervals ranging from three minutes to five days. Signal-to-noise varied from about 20 to about two, depending on atmospheric conditions, intrinsic torus brightness, and telescope used.

The scans were fit with one or two Gaussians: from the Doppler width of the one-Gaussian fit, a characteristic perpendicular ion temperature was calculated; from the total area, an intensity was derived, suitably calibrated from Jupiter and standard nebulae. The intensity data were adjusted to account for the differences in ansa, telescope, and aperture size, and the times of the east ansa data were shifted 4.9625 hours, before computing periodograms. The intensity uncertainties (which vary widely because of the different instrument configurations used) were carefully calculated (including the frequently important covariance for the two-Gaussian fits) and used in the periodicity analysis; the temperature uncertainties were not used, as they were frequently absurdly small, apparently a result of fitting non-Gaussian scans with a single Gaussian.[2] We combined [S II] $\lambda\lambda$6716,6731 data for the temperature analysis, but used only [S II] λ6731 intensities for the intensity analysis, since the intensity ratio of the two lines varies with plasma conditions. The temperatures thus obtained are given in table 1; the intensities have been previously reported (Woodward *et al.* 1994).

The periodogram with which these intensities and temperatures were examined was developed by Lomb (1976) and Scargle (1982), and extended by Horne and Baliunas (1986) and Woodward (1992); it is essentially a Fourier power spectrum (or equivalently a χ^2 sine curve fit) of unevenly spaced, unequally weighted data, which we call the *weighted Lomb-Scargle periodogram.* This analysis differs from that described in our earlier work (Woodward *et al.* 1994) in one respect: the determination of the "significance level" of the highest periodogram peak, *i.e.*, the probability that the peak is not a result of random, normally-distributed noise. Previously, we found this probability from a formula due to Horne and Baliunas (1986). This formula, however, involves assumptions about "clumping" (or lack thereof) of the data in time; therefore, following Brown (1995), we here find this probability by "shuffling" the data (randomly reassigning the intensities/temperatures to different acquisition times), calculating periodograms for these shuffled datasets, and comparing the highest peaks of the periodograms of 1000 shuffled datasets to that of the unshuffled data. Because the real intensities/temperatures and the real acquisition times are used in the shuffled data, their periodograms include the effects of non-Gaussian noise in the data and artifacts from unusual "windows" (sets of acquisition times); the excess power in the peak of the "real" periodogram,

[2]In view of the non-Gaussian line profiles of many scans, it is not clear just what the Doppler width really means. We regard it as the "typical" or "characteristic" temperature of the torus, or, more specifically, of the warm bright "ribbon" feature: images taken during the run show that there was very little [S II] λ6731 emission from the hot outer or (surprisingly) the cold inner torus (Woodward 1992).

therefore, represents genuine periodic variation in the data. (We found, in general, that these probabilities are lower than those determined by formula, although not sufficiently lower to alter the results of our earlier work.)

3. Analysis

We use here the periodogram described above to search for periodicities and quantify their statistical significance, together with "phase plots"—plots of the data modulo the proposed System IV period of 10.224 hours[3]—to examine the form of the modulation (or verify its nonexistence). Further discussion of this technique appears in Woodward *et al.* (1994) and Woodward (1992).

The [S II] λ6731 intensity periodogram is shown in fig. 1, and the [S II] $\lambda\lambda$6716,6731 temperature periodogram is shown in fig. 2; corresponding phase plots are shown in figs. 3 and 4, respectively. (Ignore, for now, the two different data symbols.) The intensity periodogram clearly shows the peak at 10.14 ± 0.06 hours reported by Woodward *et al.* (1994). (Uncertainties are at the 2σ level, as discussed in Woodward *et al.* (1994). The slightly higher peak at 7.13 h is an artifact of the 24 hour day/night modulation of our observing times, also discussed in Woodward *et al.* (1994).) The System IV period, while close, is distinctly outside of the peak; this is reflected in the small amplitude of the best-fit sine curve (fig. 3). The temperature periodogram (fig. 2) reveals a similar periodicity, with no System IV modulation evident (fig. 4).

After noting that the early data seemed organized in System IV, but that the full dataset did not, we divided the data into two subsets—before and after an arbitrary time, which we adjusted to maximize the organization of the intensities of each subset separately in System IV. The adjustment was done purely by eye, but proved to be unambiguous: 11/16/88 – 12/11/88 inclusive (97 intensity, 116 temperature scans) and 12/12/88 – 12/21/88 inclusive (60 intensity, 80 temperature scans), which we will call datasets $\mathcal{A}$ and $\mathcal{B}$, respectively; they are plotted with distinct point symbols in figs. 3 and 4, and separately in figs. 8, 9, 12, and 13. The contrast between the two is striking (although it should not be forgotten that the division was chosen specifically to *make* the contrast striking). The full data set can be described as being periodic in System IV with a phase change, or, more properly, as being *quasiperiodic* in System IV.

The intensity periodograms for datasets $\mathcal{A}$ (fig. 5) and $\mathcal{B}$ (fig. 10) both show peaks at 10.18 hours at 100.0% significance; their shifted positions (from 10.14 hours) and larger uncertainties ($\pm$0.08 and $\pm$0.24 hours, respectively) make them consistent with the System IV period of 10.224 hours. (They are also, unsurprisingly, consistent with the 10.14 ± 0.06 h period of the undivided dataset.) The periodogram of dataset $\mathcal{A}$ (fig. 5) also shows a strong component at 5.10 hours

[3]A better subcorotational period to use for comparison might be the 10.214 h found by Brown (1995), rather than the 10.224 h of System IV, but the difference is insignificant over a five week run, so we use System IV out of convenience and familiarity.

(the second harmonic of the 10.18 h period), which remains significant (100.0%) after the removal of the primary periodicity by prewhitening (fig. 6). [4] The phase plot of dataset $\mathcal{A}$ (fig. 8) clearly reflects this second harmonic, showing a maximum at $\sim 130°$ and a weaker one at $\sim 300°$; the phase plot of dataset $\mathcal{B}$ (fig. 12) shows a maximum at $\sim 350°$ and a (statistically not significant) hint of a second maximum as well. (The cluster of four points from 0° to 60° at about 260 Rayleighs in fig. 12 are from the first night of dataset $\mathcal{B}$, possibly representing a transition process.) In both cases the modulation (peak-to-peak) is comparable to the average value.

The temperature periodograms differ strikingly from the intensity periodograms. Dataset $\mathcal{A}$ shows no significant temperature periodicity whatever (fig. 7), and the phase plot (fig. 9) concurs (with perhaps a weak modulation at 5.112 hours); dataset $\mathcal{B}$, however, shows a clear, significant (99.97%) periodicity at 10.06 ± 0.24 hours (fig. 11), and the phase plot (fig. 13) shows a temperature enhancement approximately anticorrelated with intensity (fig. 12).

We computed Spearman rank-order correlation coefficients r_s of intensities *vs.* temperatures for the two datasets; the results confirm what the phase plots suggest to the eye. For dataset $\mathcal{A}$, $r_s = -0.019$, corresponding to a probability of just 69% (against the null hypothesis of no anti-correlation), while for dataset $\mathcal{B}$, $r_s = -0.298$, corresponding to a probability of 99%, *i.e.* there is a significant anticorrelation between intensity and temperature in the later data, but not the earlier. (The 10.06 ± 0.24 hour periodicity of dataset $\mathcal{B}$ temperatures makes them consistent with the System III modulation in Doppler-width temperatures reported by Brown (1995) as well, but, if this is the same System III temperature modulation described by Schneider and Trauger (1995) and Brown (1995), it is surprising that it does not appear in dataset $\mathcal{A}$.)

4. Interpretation

Since the discovery of subcorotational periodicities in the plasma torus, the physical mechanism(s) for them have been a mystery; the results we present here do not resolve this mystery, but do provide a few clues. The smaller intensity peak in fig. 8 (dataset $\mathcal{A}$) falls near the longitude of the peak in fig. 12 (dataset $\mathcal{B}$), suggesting that, rather than a single feature that is usually fixed in System IV longitude but occasionally moves, there are two features, both fixed at different longitudes in System IV but occasionally changing amplitudes. The anticorrelation of intensity and temperature in dataset $\mathcal{B}$ (figs. 12 and 13) suggests that the dominant System IV feature in that dataset may be a temperature-related density (and therefore emission) enhancement. (This may also explain why Brown (1995) saw an overall intensity enhancement concurrent with the System IV phase change during his run, while we did not. His data were acquired with a long-slit spectrograph, and therefore excluded high-latitude emission, which makes up a larger fraction of the total emisson we see at higher temperatures than at lower.) The absence of an intensity/temperature

[4] No significant System III period remains in this prewhitened periodogram, which is consistent with our earlier analysis of the full dataset (Woodward *et al.* 1994).

anticorrelation in dataset $\mathcal{A}$, however, shows that its dominant System IV feature is fundamentally different.

A periodicity can only be detected (and arguably only has meaning) if there is some distinctive feature, such as an emission intensity enhancement or depletion, moving or otherwise varying with that period. It is now clear that features organized in System IV do not remain constant (or even consistently present) over time, and indeed can on occasion change radically from one night to the next: this behavior was first evident in the *Voyager* nKOM data (Daigne and Leblanc 1986), was later shown dramatically by Brown (1995), is evident in the recent *Voyager* HOM analysis (Kaiser *et al.* 1996) (where the sources appear fixed in System III but modulated in System IV), and is also seen in the present work, where the two System IV organized features appear to be not only spatially distinct but physically different. The transient nature of these System IV-organized features, together with the large range of their radial positions in the torus, indicate that while System IV is a permanent, global property in the torus (and perhaps the inner magnetosphere), it has thus far manifested itself only in the behavior of long-lived but impermanent azimuthal features that appear from time to time in the torus; the underlying mechanism of System IV, whatever it may be, has yet to be directly observed.

There are, broadly speaking, two theories about the origin of the 3% corotational lag. The most obvious explanation, put forth by Hill and others (Hill 1979, Hill 1980, Pontius and Hill 1982, Huang and Hill 1989), is that (some of) the ions are themselves lagging corotation. Indeed, corotational lag is expected near Io's orbit, where fresh plasma is created from the cloud of neutral atoms and molecules surrounding Io: the newly-created plasma generates Birkeland currents connecting the plasma and the Jovian ionosphere, and the $\mathbf{E}$ field thus produced gives rise to an $\mathbf{E} \times \mathbf{B}$ drift that slows the plasma (Pontius and Hill 1982, Pontius 1995). The other theory, by Dessler and others (Dessler 1985, Sandel and Dessler 1988, Yang and Dessler 1991), holds that the Jovian magnetic field has two components rotating at different speeds. (Such a dual magnetic rotational periodicity is known to exist in the Sun (Hoeksema and Scherrer 1987) and possibly in Saturn (Dessler 1985).) Distinct features in the more slowly rotating part of the magnetic field (for which Dessler (Sandel and Dessler 1988) created the provisional System IV longitudinal system used in this paper) would naturally exhibit periodicity at the slower period. This theory is appealing because of its broader scope; it also accounts for the two distinct periods seen in the EUV data analyzed by Sandel and Dessler (1988), and in the optical data analyzed by Woodward *et al.* (1994) and Brown (1995). Details of the slower magnetic "component" and its effect on the torus, however, are not given.

Obvious candidates for System IV-organized features are regions of unusually dense or rarified plasma that are subcorotating—either freshly-injected plasma that has not yet been brought up to corotation, or variations in a uniformly subcorotating torus. Plasma lags have been observed directly through measurements of the Doppler shifts of the [S II] $\lambda\lambda$6716,6731 lines, but vary from 2%–10% (Brown 1983), and are localized near Io (Brown 1994); *in situ* measurements by *Ulysses* also imply lags of up to 10% near Io (Kellogg *et al.* 1993). Likewise, the nKOM radiation sources observed by *Voyager* (Kaiser and Desch 1980) show a variable lag (Daigne and Leblanc 1986), and the nKOM radiation seen by *Ulysses* appears to originate from several sources, each with its own corotational lag (Reiner *et al.* 1993). But a corotational lag must be constant in period in order for it to be detected in a periodogram; the observed plasma lags and nKOM source lags are therefore unlikely to give rise to the persistent 3% subcorotational periodicity. Moreover, Brown (1995) reports that the 3% subcorotational periodicity, unlike the direct plasma subcorotation, is present at all (line-of-sight) radial distances from 5.875 to 6.75 R_J.

If the plasma itself is not subcorotating, however, (except near Io's orbit) then what is? The traditional plasma drifts and waves cannot distinguish east from west (hence we would expect to see a supercorotational periodicity as well); their speeds, moreover, vary with plasma density, and thus would not remain a constant 3% slower than corotation. The idea of some subcorotating magnetic field feature is appealing, as it would affect the entire torus; indeed, although Kaiser *et al.* (1996) interpret their System IV HOM modulation as arising from refraction by a System IV-organized plasma enhancement, we note that the HOM sources are generally believed to be located at high Jovian magnetic latitudes, where Dessler (1985) predicts subcorotational magnetic effects to be strongest, by analogy with the Sun. However, if the magnetic field at the torus were subcorotating, the plasma itself should subcorotate as well—indeed, one could no longer properly call it "subcorotating"—but Brown (1995) reports that this is not the case.

The present work addresses the hypothesis that a secondary magnetic field component is somehow responsible for System IV (Dessler 1985, Sandel and Dessler 1988). If, in the simplest case, a wave of local magnetic field strength enhancement moves slowly westward through the torus, it can create a subcorotating intensity enhancement without actual plasma subcorotation, but we would expect to see correlated temperature enhancements as well, from the conservation of the first adiabatic invariant; instead we see no significant temperature change (dataset $\mathcal{A}$) or a temperature *decrease* (dataset $\mathcal{B}$). Furthermore, if a magnetic field component were causing the enhancements by any means, that component would have to change phase quickly from time to time, or be such as to cause plasma torus properties to change phase quickly. Thus, the source of System IV requires a more exotic magnetic field component, or else some altogether different mechanism.

Acknowledgments

We wish to thank the staff of the National Solar Observatory for their generous support during the observational program. We also thank Ron Oliversen for observational assistance and general help with instrument preparation. This work was carried out with support from the National Aeronautics and Space Administration through grant NAGW-3319 and contract NAS 5-30131.

REFERENCES

Brown, M. E. 1994. Observation of mass loading in the Io plasma torus. *Geophys. Res. Lett.*, **21**, 847–850.

Brown, M. E. 1995. Periodicities in the Io plasma torus. *J. Geophys. Res.*, **100**, 21683–21695.

Brown, R. A. 1983. Observed departure of the Io plasma torus from rigid corotation with Jupiter. *ApJ*, **268**, L47–L50.

Daigne, G. and Y. Leblanc 1986. Narrow-band Jovian kilometric radiation: Occurence, polarization, and rotation period. *J. Geophys. Res.*, **91**, 7961–7969.

Dessler, A. J. 1985. Differential rotation of the magnetic fields of gaseous planets. *Geophys. Res. Lett.*, **12**, 299–302.

Hill, T. W. 1979. Inertial limit on corotation. *J. Geophys. Res.*, **84**, 6554–6558.

Hill, T. W. 1980. Corotational lag in Jupiter's magnetosphere: A comparison of observation and theory. *Science*, **207**, 301–302.

Hoeksema, J. T. and P. H. Scherrer 1987. Rotation of the coronal magnetic field. *ApJ*, **318**, 428–436.

Horne, J. H. and S. L. Baliunas 1986. A prescription for period analysis of unevenly sampled time series. *ApJ*, **302**, 757–763.

Huang, T. S. and T. W. Hill 1989. Corotational lag of the jovian atmosphere, ionosphere, and magnetosphere. *J. Geophys. Res.*, **94**, 3761–3765.

Kaiser, M. L. and M. D. Desch 1980. Narrow-band Jovian kilometric radiation: A new radio component. *Geophys. Res. Lett.*, **7**, 389–392.

Kaiser, M. L., M. D. Desch, and M. E. Brown 1996. Evidence for an Io plasma torus influence on high-latitude Jovian radio emission. *J. Geophys. Res.*, , 13–18.

Kellogg, P. J., K. Goetz, R. L. Howard, S. J. Monson, A. Balogh, and R. J. Forsyth 1993. Measurements of direct current electric fields and plasma flow in Jupiter's magnetosphere. *J. Geophys. Res.*, **98**, 13307–13314.

Lomb, N. R. 1976. Least-squares frequency analysis of unequally spaced data. *Ap&SS*, **39**, 447–462.

Pontius, Jr., D. H. 1995. Implications of variable mass loading in the Io torus: The Jovian flywheel. *J. Geophys. Res.*, **100**, 19531–19539.

Pontius, Jr., D. H. and T. W. Hill 1982. Departure from corotation of the Io plasma torus: Local plasma production. *Geophys. Res. Lett.*, **9**, 1321–1324.

Reiner, M. J., J. Fainberg, R. G. Stone, M. L. Kaiser, M. D. Desch, R. Manning, P. Zarka, and B.-M. Pedersen 1993. Source characteristics of Jovian narrow-band kilometric radio emissions. *J. Geophys. Res.*, **98**, 13163–13176.

Roesler, F. L., F. Scherb, and R. J. Oliversen 1984. Periodic intensity variations in [S III] 9531Å emission from the Jupiter plasma torus. *Geophys. Res. Lett.*, **11**, 128–130.

Sandel, B. R. and A. J. Dessler 1988. Dual periodicity of the Jovian magnetosphere. *J. Geophys. Res.*, **93**, 5487–5504.

Scargle, J. D. 1982. Studies in astronomical time series analysis. II. Statistical aspects of spectral analysis of unevenly spaced data. *ApJ*, **263**, 835–853.

Schneider, N. M. and J. T. Trauger 1995. The Structure of the Io Torus. *ApJ*, **450**, 450–462.

Woodward, Jr., R. C. 1992. *The Sulfur Emission and Periodicity of the Jupiter Plasma Torus in 1988*. PhD thesis, University of Wisconsin—Madison.

Woodward, Jr., R. C., F. Scherb, F. L. Roesler, and R. J. Oliversen 1994. Periodic intensity variations in sulfur emissions from the Io plasma torus.ls

Icarus, **111**, 45–64.

Yang, Y. S. and A. J. Dessler 1991. Is System IV independent of System III? *J. Geophys. Res.*, **96**, 3819–3824.

This preprint was prepared with the AAS LaTeX macros v4.0.

Table 1. Temperatures from [S II] emission linewidths

Date	S	A	L	Time	$T_\perp$	Date	S	A	L	Time	$T_\perp$	Date	S	A	L	Time	$T_\perp$
11/16	A	E	r	5:13	33.6	11/24	M	E	r	8:50	45.5	12/13	A	E	r	9:35	40.3
11/17	A	E	r	3:44	25.8					9:37	44.4					10:07	44.1
				5:32	58.5				b	9:51	37.1				b	10:20	48.0
				6:41	46.6	11/31	M	W	r	5:25	42.5				r	10:30	57.3
				7:24	36.1				b	5:41	33.9					10:56	31.6
				7:55	20.0	12/02	M	W	r	3:05	32.3					11:08	36.6
				8:08	62.8					3:16	44.2	12/14	A	W	r	3:04	66.3
				9:15	20.5				b	4:02	47.8				b	4:03	26.4
11/20	A	E	r	8:22	30.5				r	4:28	58.2				r	4:19	53.1
11/21	A	E	r	5:34	16.0					4:40	45.0					4:53	73.3
				6:02	58.1				b	5:18	51.8				b	5:20	81.6
		W		6:21	30.3				r	5:53	50.9				r	5:33	25.3
		E		6:50	49.9				b	9:35	31.5					7:04	125.0
				7:59	84.1				r	10:00	57.5					7:52	96.0
				8:37	48.7					10:53	46.0					9:15	83.2
		W		8:53	26.4	12/03	M	E	r	4:39	58.9					9:28	55.5
				9:05	61.9				b	4:55	66.8	12/15	A	E	r	1:46	33.4
		E		9:39	48.6				r	5:09	47.2				b	2:26	27.6
				9:51	51.6					7:01	40.3				r	2:57	48.2
				10:02	44.3				b	7:21	42.8	12/16	A	E	r	2:00	26.8
		W		10:19	84.0				r	7:35	45.4					2:13	36.2
				10:36	97.9					8:42	39.8					2:38	87.8
		E		10:51	18.6					10:17	40.5					2:50	62.1
				11:02	27.4	12/04	A	W	b	9:58	11.7					3:08	50.7
				11:16	10.4				r	10:34	47.9					3:20	58.8
				11:51	33.1					10:48	46.4			W		3:36	31.7
		W		12:08	18.0					11:02	16.8					4:27	66.6
				12:21	43.9					11:15	43.9				b	4:42	40.8
11/22	M	E	r	6:42	45.9					11:27	36.1				r	5:06	84.3
		W		7:14	40.4	12/05	A	E	r	2:05	51.4					6:03	63.1
				7:27	49.5				b	2:22	31.5			E		6:22	65.1
		E		8:14	49.1				r	2:43	34.7					7:10	47.5
				8:25	60.8				b	3:30	27.6				b	7:24	46.4
				8:36	42.6				r	3:41	71.0				r	7:39	37.8
				8:47	61.5					3:52	99.3					8:04	56.2
				8:59	61.7					4:08	46.6					8:17	51.6

Table 1—Continued

Date	S	A	L	Time	$T_\perp$	Date	S	A	L	Time	$T_\perp$	Date	S	A	L	Time	$T_\perp$
11/22	M	W	r	9:37	69.3	12/05	A	E	r	4:22	66.6	12/16	A	E	r	8:30	38.3
				9:48	63.0					4:35	47.7				b	8:44	20.5
				9:59	51.4					4:48	56.7				r	8:54	40.8
				10:25	56.2				b	5:03	48.4			W	b	9:25	78.5
				10:36	52.1					5:14	63.3				r	9:38	98.9
				10:47	49.9	12/11	M	W	r	3:12	49.2	12/18	A	W	r	1:52	103.9
				10:57	47.9				b	3:40	56.0			E		2:17	36.4
				11:13	47.0				r	3:54	46.4				b	2:35	48.7
				11:23	49.9					5:37	42.0			W	r	3:46	60.9
11/23	M	W	r	8:29	29.5				r	6:49	71.0				b	4:27	56.3
				8:48	39.5				b	7:04	108.2				r	4:41	39.1
				9:24	31.1				r	7:14	50.7				b	5:20	31.7
				9:42	56.4					9:33	56.8				r	5:34	27.9
				11:32	45.1					10:14	42.9					8:38	31.6
				11:44	70.2	12/12	M	E	r	2:59	53.5					9:10	52.2
				12:07	35.2				b	3:17	49.6				b	9:46	22.0
				12:19	52.7				r	3:26	45.7				r	9:58	97.3
				12:31	43.6					3:39	46.3	12/20	M	W	r	4:15	110.0
11/24	M	W	r	4:44	41.0				b	3:56	44.8					6:25	61.1
			b	5:25	31.2				r	4:07	39.3				b	6:39	95.6
			r	5:38	37.7					5:19	38.8				r	6:51	66.7
			b	5:51	40.5				b	5:32	38.5	12/21	M	E	r	3:41	73.7
			r	6:01	45.5				r	5:42	51.4				b	4:00	75.2
			b	6:14	35.2				b	9:47	53.5				r	4:10	93.7
		E	r	7:27	54.7				r	9:57	54.4					4:44	83.0
				7:39	56.8				b	11:01	58.8			W		5:33	54.1
			b	8:00	56.2				r	11:10	66.9					7:15	71.5
			r	8:12	59.9	12/13	A	E	r	9:11	36.4					8:46	65.6
				8:23	59.3				b	9:26	24.6					9:56	68.1
			b	8:39	69.5												

Note. — Dates and times are UT at the beginning of each scan; temperatures are in eV. Remaining columns are as follows:

S Telescope: M = Main; A = Auxiliary

A Ansa: E = East (approaching); W = West (receding)

L Emission line: r = 6731Å; b=6716Å

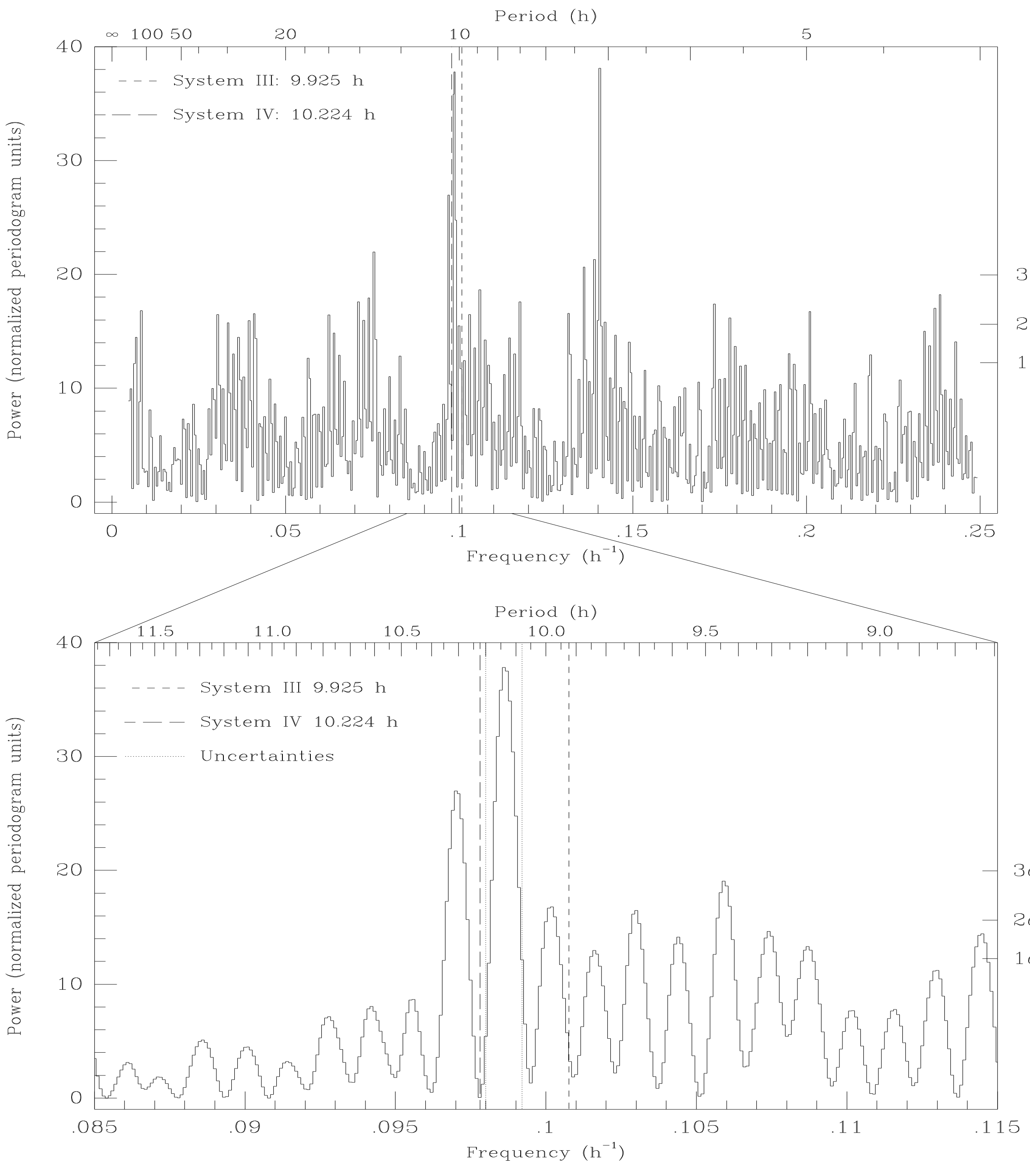

Fig. 1.— Periodogram of [S II] $\lambda 6731$ intensities for 11/16/88–12/21/88 (full dataset), showing periodicity at 10.14 ± 0.06 h. The 1σ, 2σ, and 3σ marks in this and the following periodograms are 68.26%, 95.44%, and 99.74% probability levels, respectively, that the highest peak is not a result of random noise.

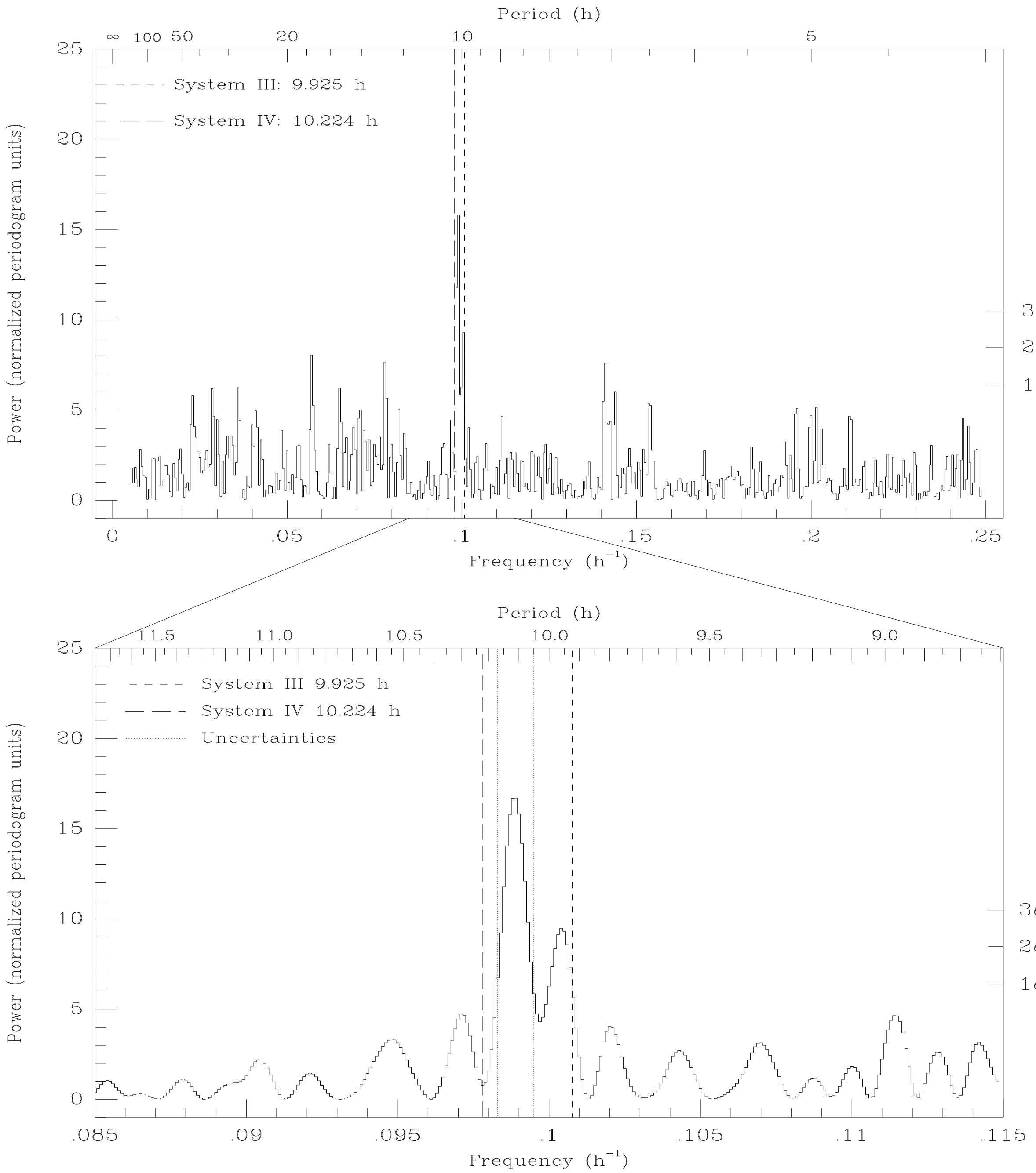

Fig. 2.— Periodogram of [S II] $\lambda\lambda$6716,6731 temperatures for 11/16/88–12/21/88 (full dataset). Highest peak is at $10.11 \pm 0.06\,$h.

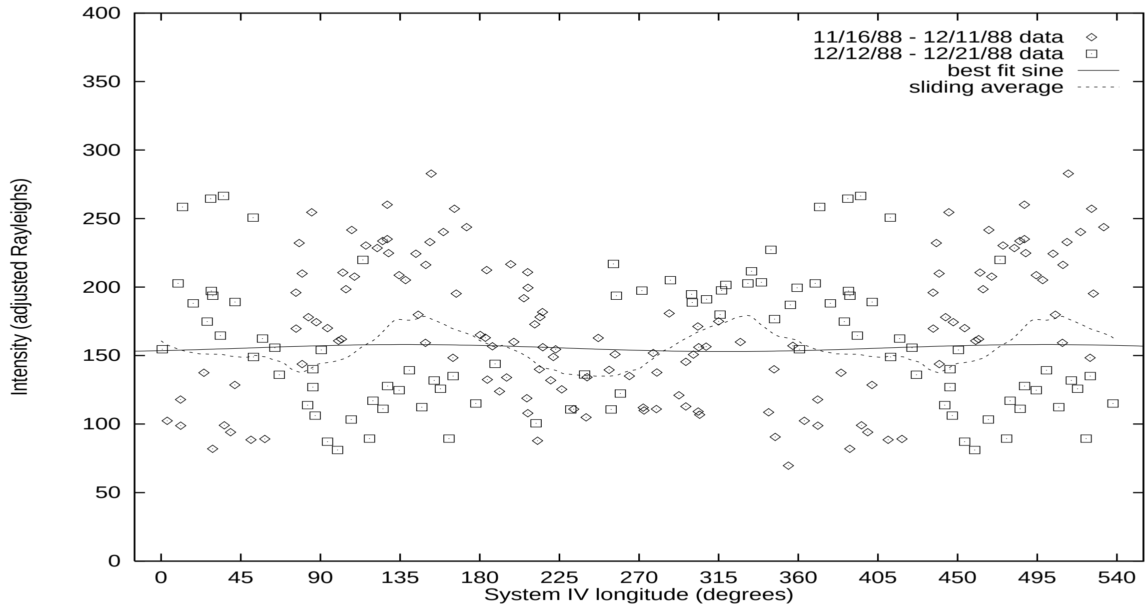

Fig. 3.— Phase plot of [S II] $\lambda6731$ intensities for 11/16/88–12/21/88 (full dataset) in the proposed System IV longitude system. The almost flat solid curve is *not* a baseline, but the best-fit sine curve to the data. The sliding average in this and the following phase plots is over a $60°$ wide quadratic window. Different symbols are used for datasets $\mathcal{A}$ and $\mathcal{B}$, for comparison with later figures.

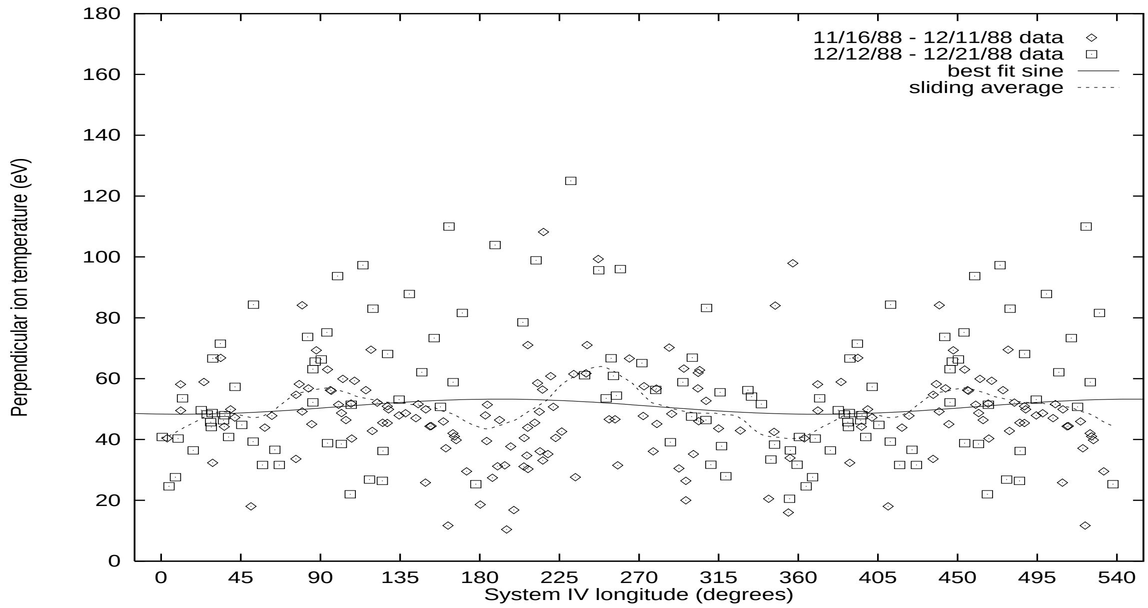

Fig. 4.— Phase plot of [S II] $\lambda\lambda6716,6731$ temperatures for 11/16/88–12/21/88 (full dataset) in the proposed System IV longitude system, with best-fit sine curve and $60°$ sliding average.

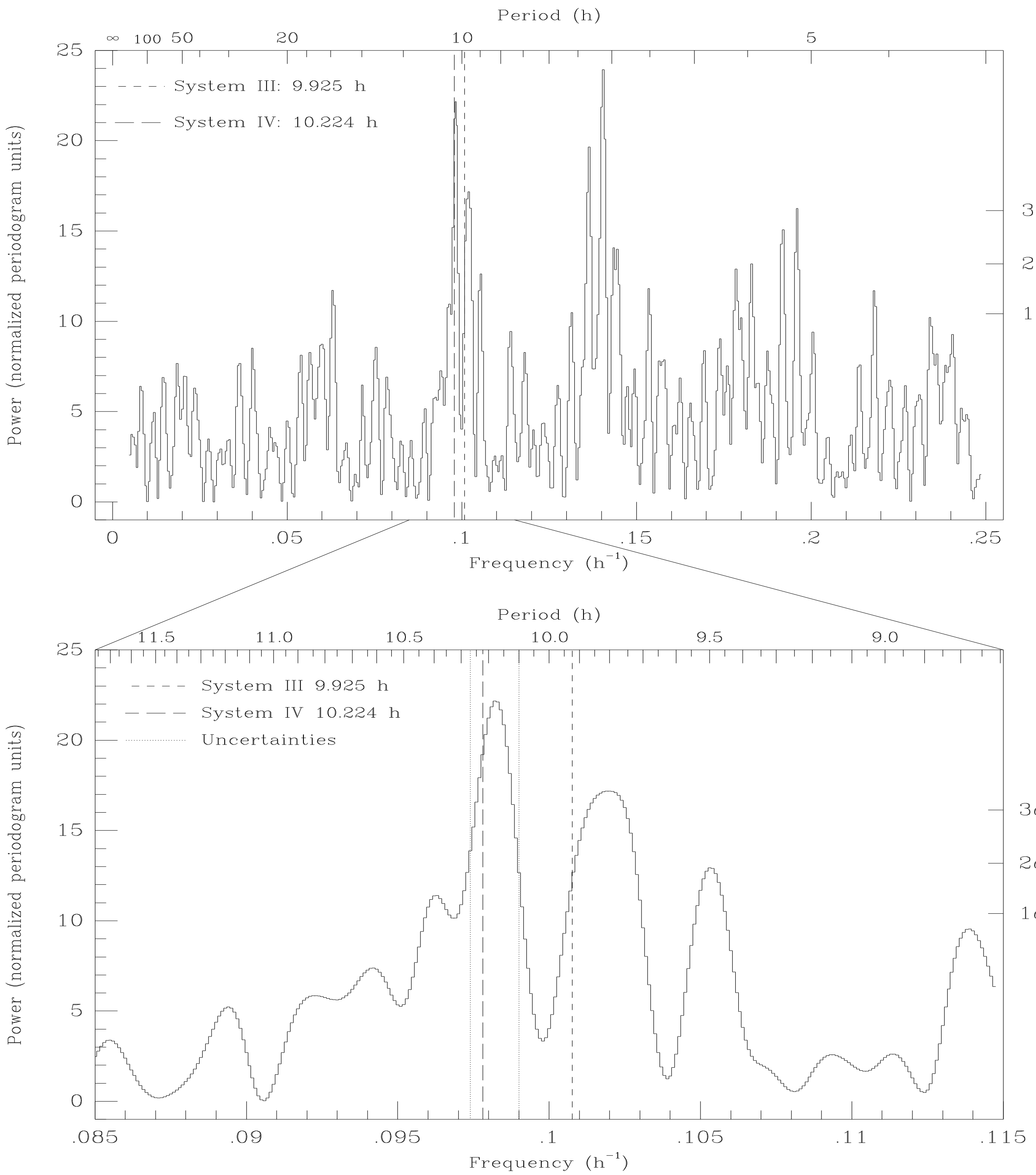

Fig. 5.— Periodogram of [S II] λ6731 intensities for 11/16/88–12/11/88 (dataset $\mathcal{A}$). Highest peak is at 10.18 ± 0.08 h.

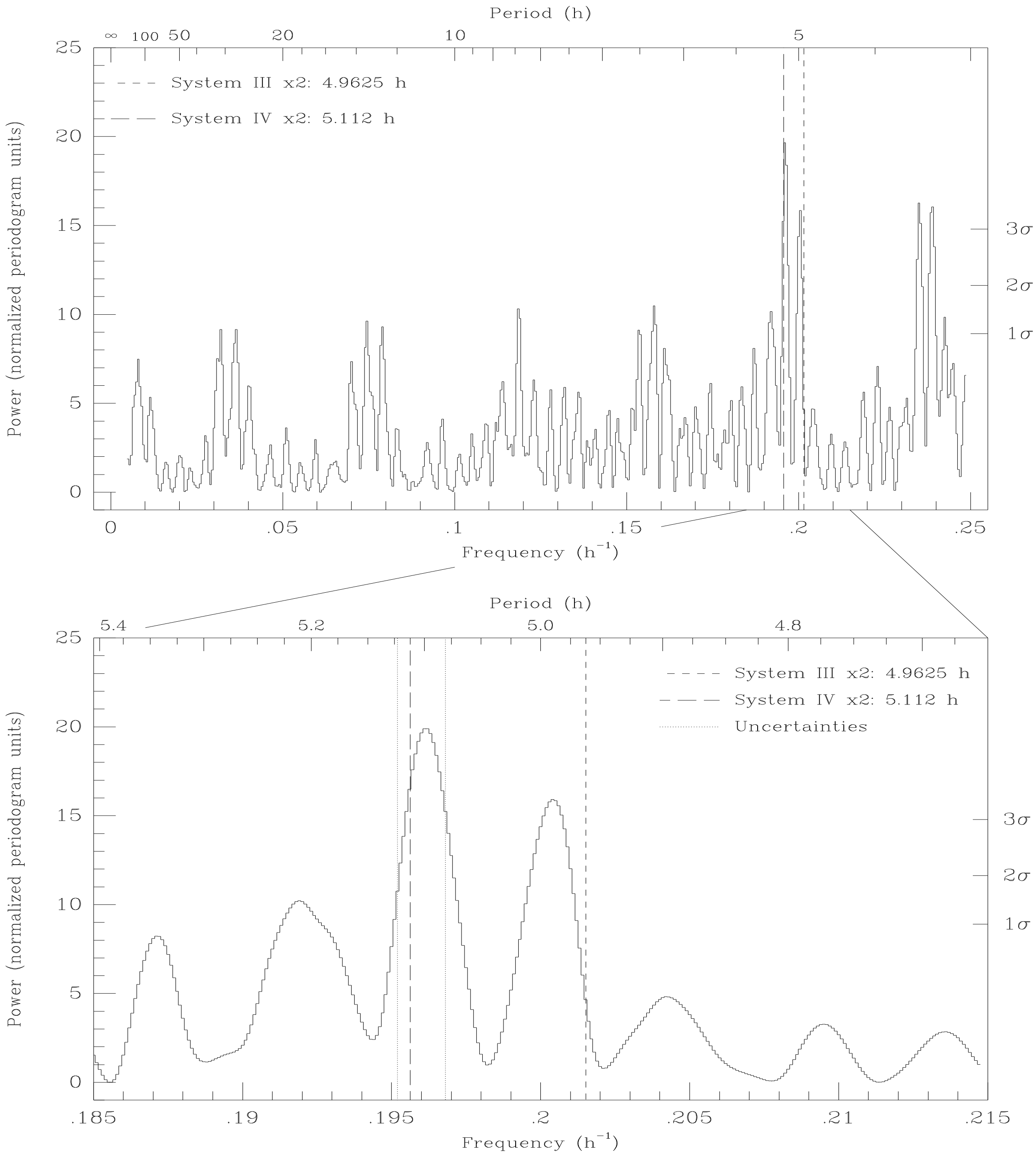

Fig. 6.— Periodogram of [S II] λ6731 intensities for 11/16/88–12/11/88 (dataset $\mathcal{A}$), after subtracting out (prewhitening) the 10.18 h period. Highest peak is at 5.10 ± 0.08 h.

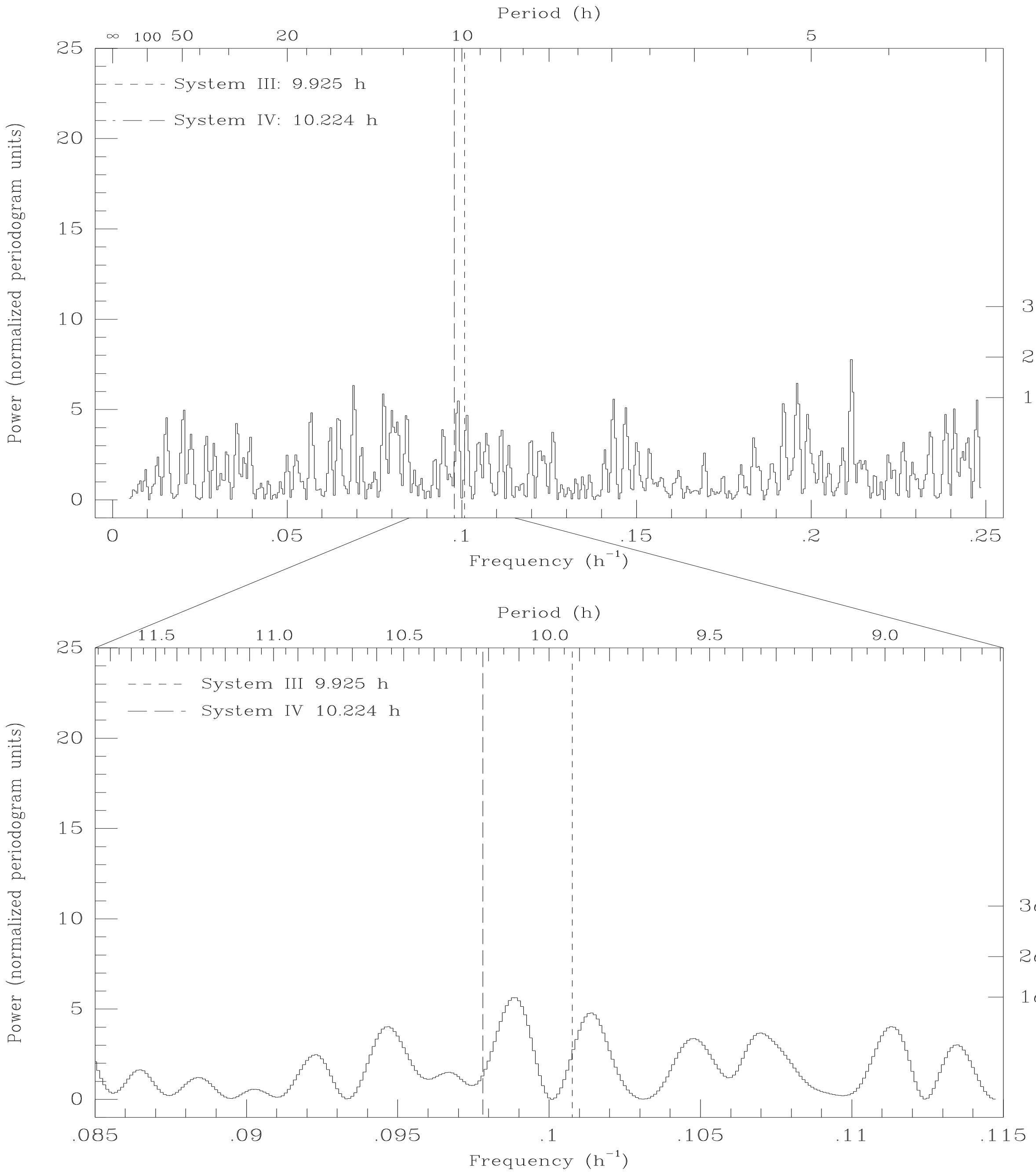

Fig. 7.— Periodogram of [S II] $\lambda\lambda6716,6731$ temperatures for 11/16/88–12/11/88 (dataset $\mathcal{A}$).

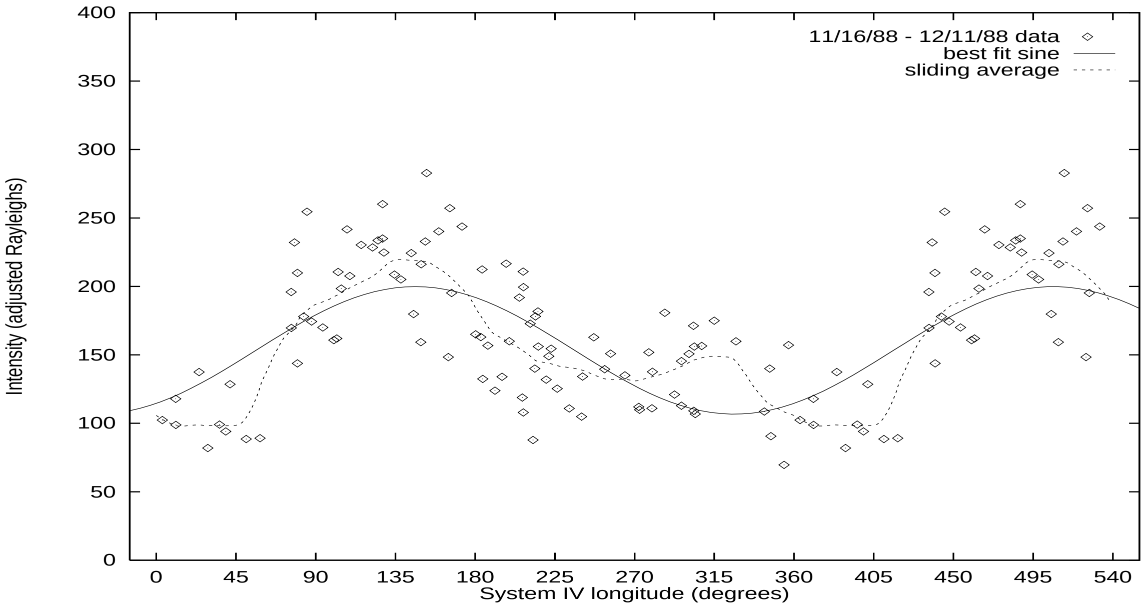

Fig. 8.— Phase plot of [S II] λ6731 intensities for 11/16/88–12/11/88 (dataset $\mathcal{A}$) in the proposed System IV longitude system, with curves showing best-fit sine and 60° sliding average.

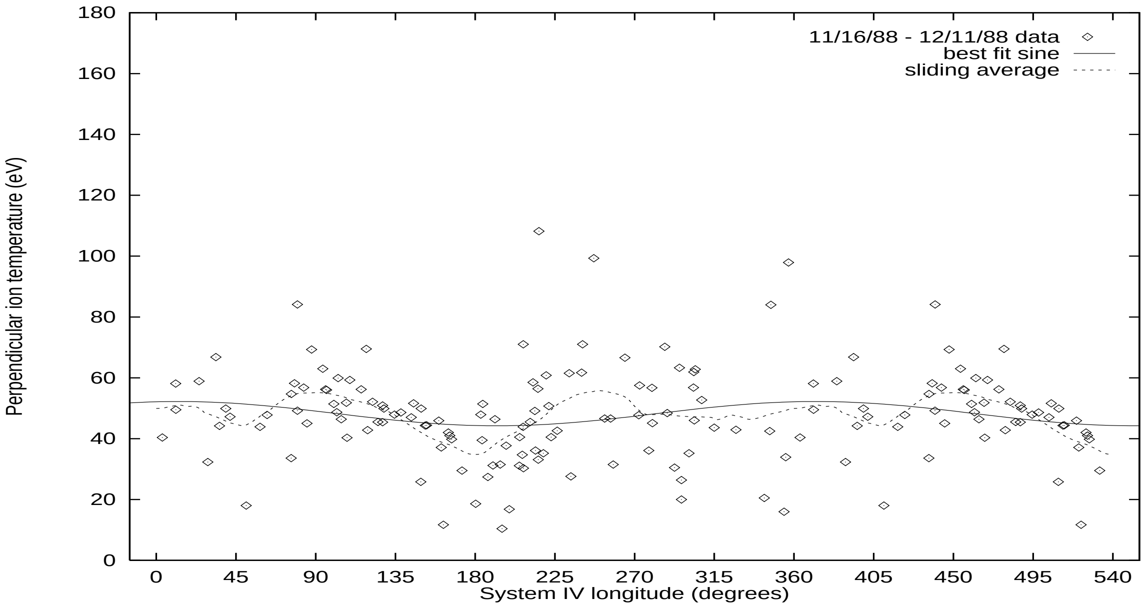

Fig. 9.— Phase plot of [S II] $\lambda\lambda$6716,6731 temperatures for 11/16/88–12/11/88 (dataset $\mathcal{A}$) in the proposed System IV longitude system, with curves showing best-fit sine and 60° sliding average.

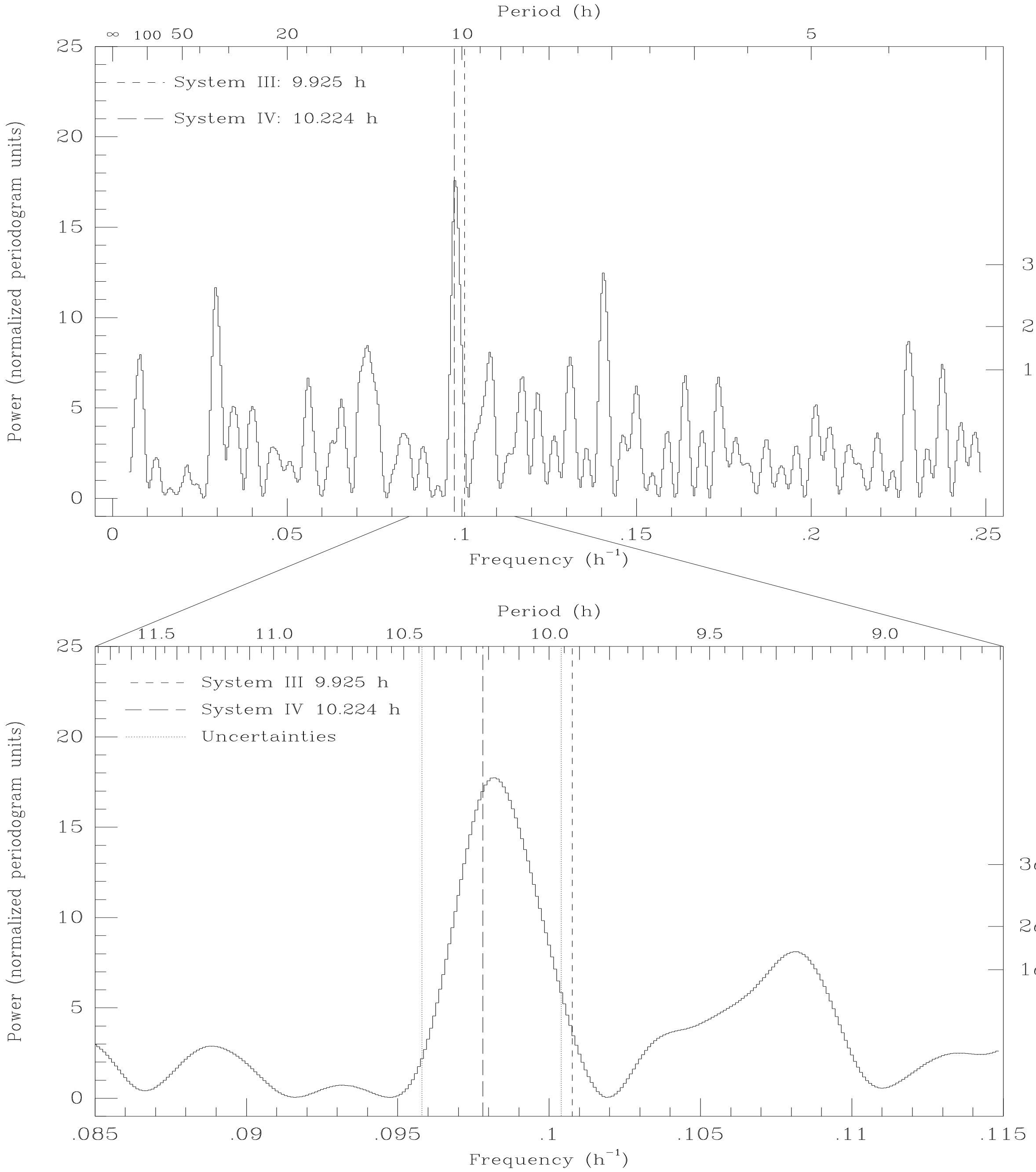

Fig. 10.— Periodogram of [S II] λ6731 intensities for 12/12/88–12/21/88 (dataset $\mathcal{B}$). Highest peak is at 10.18 ± 0.24 h.

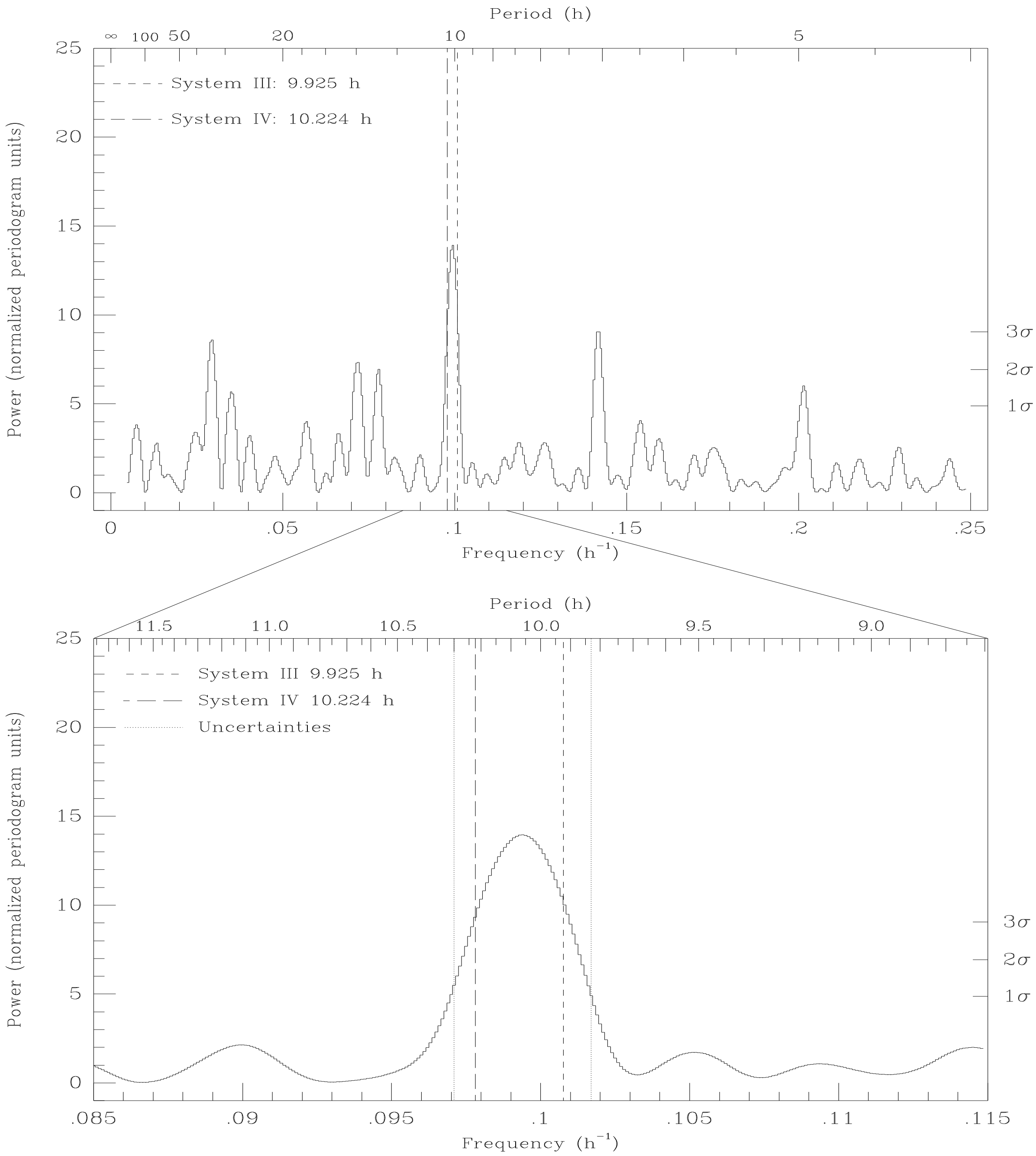

Fig. 11.— Periodogram of [S II] $\lambda\lambda$6716,6731 temperatures for 12/12/88–12/21/88 (dataset $\mathcal{B}$). Highest peak is 10.07 ± 0.24 h.

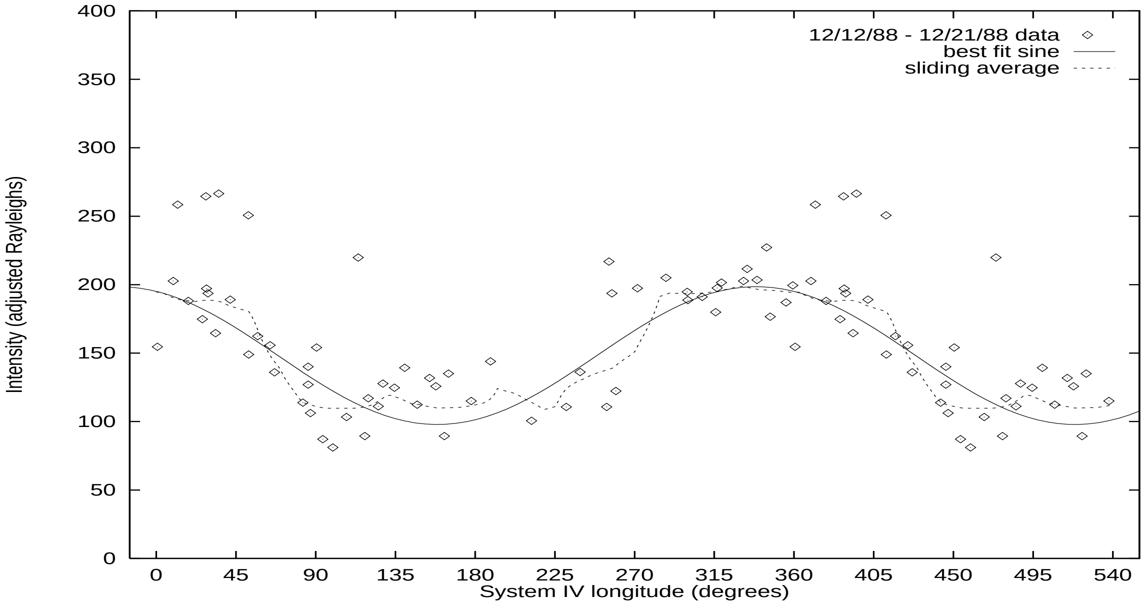

Fig. 12.— Phase plot of [S II] λ6731 intensities for 12/12/88–12/21/88 (dataset $\mathcal{B}$) in the proposed System IV longitude system, with curves showing best-fit sine and 60° sliding average.

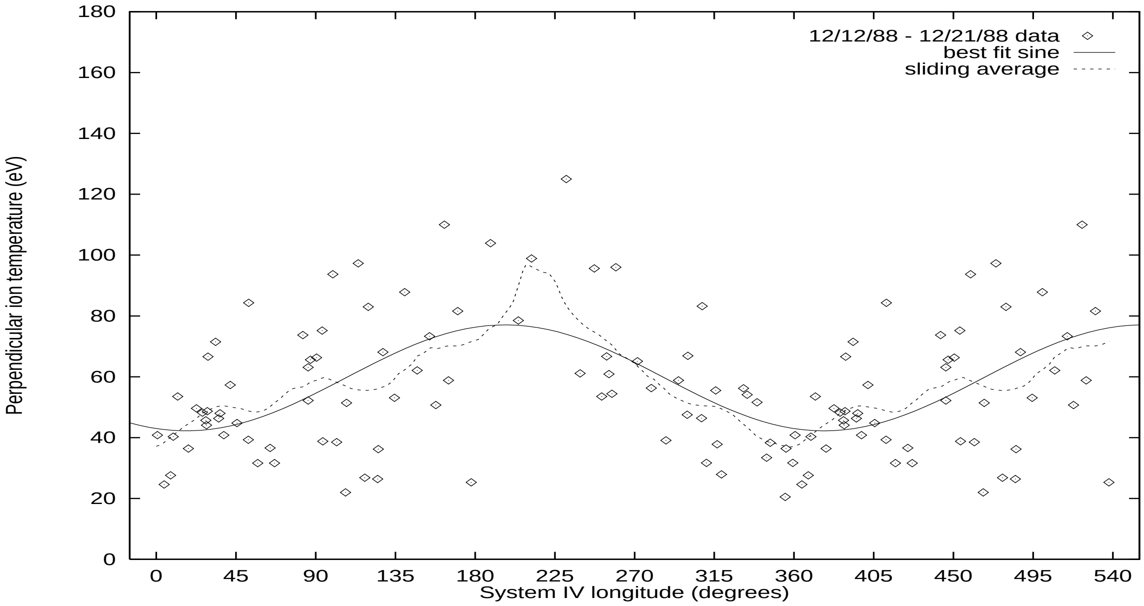

Fig. 13.— Phase plot of [S II] $\lambda\lambda$6716,6731 temperatures for 12/12/88–12/21/88 (dataset $\mathcal{B}$) in the proposed System IV longitude system, with curves showing best-fit sine and 60° sliding average.